Biochemical and Biophysical Research Communications 439 (2013) 533–538

Contents lists available at ScienceDirect

Biochemical and Biophysical Research Communications

journal homepage: www.elsevier.com/locate/ybbrc

The crystal structure of a novel phosphopantothenate synthetase from the hyperthermophilic archaea, *Thermococcus onnurineus* NA1

Min-Kyu Kim [a], Young Jun An [a], Sun-Shin Cha [a,b,c,*]

[a] Marine Biotechnology Research Division, Korea Institute of Ocean Science and Technology, Ansan 426-744, Republic of Korea
[b] Ocean Science and Technology School, Korea Maritime University, Pusan 606-791, Republic of Korea
[c] Department of Marine Biotechnology, University of Science and Technology, DaeJeon 305-333, Republic of Korea

ARTICLE INFO

Article history:
Received 30 August 2013
Available online 8 September 2013

Keywords:
Coenzyme A biosynthesis
Archaea
Phosphopantothenate synthetase
Crystal structure of TON1374
Crystal structure of TON1374/ATP complex

ABSTRACT

Pantothenate is the essential precursor of coenzyme A (CoA), a fundamental cofactor in all aspects of metabolism. In bacteria and eukaryotes, pantothenate synthetase (PS) catalyzes the last step in the pantothenate biosynthetic pathway, and pantothenate kinase (PanK) phosphorylates pantothenate for its entry into the CoA biosynthetic pathway. However, genes encoding PS and PanK have not been identified in archaeal genomes. Recently, a comparative genomic analysis and the identification and characterization of two novel archaea-specific enzymes show that archaeal pantoate kinase (PoK) and phosphopantothenate synthetase (PPS) represent counterparts to the PS/PanK pathway in bacteria and eukaryotes. The TON1374 protein from *Thermococcus onnurineus* NA1 is a PPS, that shares 54% sequence identity with the first reported archaeal PPS candidate, MM2281, from *Methanosarcina mazei* and 91% sequence identity with TK1686, the PPS from *Thermococcus kodakarensis*. Here, we report the apo and ATP-complex structures of TON1374 and discuss the substrate-binding mode and reaction mechanism.

1. Introduction

Coenzyme A (CoA) is an essential cofactor in numerous metabolic and energy-yielding pathways and is involved in the regulation of key metabolic enzymes. CoA is also the source of 4′-phosphopantetheine, which is required in several biosynthetic pathways, including fatty acid and polyketide syntheses [1]. The pathways for CoA biosynthesis have been studied in a variety of bacteria and eukaryotes, which utilize a common enzymatic pathway. CoA is synthesized from pantothenate via five successive enzymatic reactions: pantothenate kinase (PanK), 4′-phosphopantothenoylcysteine synthetase (PPCS), 4′-phosphopantothenoylcysteine decarboxylase (PPCDC), 4′-phosphopantetheine adenylyltransferase (PPAT), and dephospho-CoA kinase (DPCK).

Although many animals rely on exogenous pantothenate to initiate CoA biosynthesis [2], microorganisms and plants can synthesize the CoA precursor, pantothenate, from 2-oxoisovalerate and β-alanine [3] in a three-step pathway catalyzed by ketopantoate hydroxymethyltransferase (KPHMT), ketopantoate reductase (KPR), and pantothenate synthetase (PS).

There is abundant information on CoA biosynthesis in bacteria and eukaryotes, whereas the corresponding pathway in archaea has not been well described. In particular, almost all archaeal genomes lack genes corresponding to PS and PanK. After strong candidates for archaeal PS and PanK were suggested based on comparative genomics and the identification of a novel PS from *Methanosarcina mazei*[4,5], two novel enzymes, pantoate kinase (PoK, TK2141) and 4′-phosphopantothenate synthetase (PPS, TK1686), were identified and characterized [6]. PoK and PPS were demonstrated to convert pantoate to 4′-phosphopantothenate, replacing the missing PS/PanK pathway in *Thermococcus kodakarensis*[6]. The classical PS/PanK system in bacteria and eukaryotes involves condensation with β-alanine prior to phosphorylation, but the PoK/PPS system in archaea encompasses novel enzyme reactions: the phosphorylation of pantoate (PoK) [7], followed by the condensation of 4-phosphopantoate and β-alanine (PPS) [8]. Homologs of genes encoding PS and PPS are distributed in almost all archaeal genomes (Fig. S1).

The TON1374 protein from *Thermococcus onnurineus* NA1 is a homolog of PPS (EC 6.3.2.26, 4-phosphopantoate-β-alanine ligase) and shares 91% amino acid sequence identity with TK1686. TON1374 belongs to Pfam family PF02006 (DUF137) [9,10] and the COG1701 family [11], which have been suggested as the best candidates for the missing steps leading from pantoate to 4′-phosphopantothenate in archaeal CoA biosynthesis [4,5]. Here, we report the crystal structures of novel archaea-specific phosphopantothenate synthetase in both the apo and ATP-bound forms. The structure of ATP-bound TON1374 suggests the

* Corresponding author. Address: Marine Biotechnology Research Division, Korea Institute of Ocean Science and Technology, Ansan, P.O. Box 29, Seoul 425-600, Republic of Korea. Fax: +82 31 406 2495.
E-mail address: chajung@kiost.ac (S.-S. Cha).

0006-291X/$ - see front matter © 2013 Elsevier Inc. All rights reserved.
http://dx.doi.org/10.1016/j.bbrc.2013.09.008

ATP-enzyme interactions and reveals that the core domain of TON1374, which contains the ATP-binding site is similar to the nucleotide-binding domains of oxalyl-CoA decarboxylase (OXC) [12], Sir2 homolog protein [13], and carboxyethylarginine synthase (CEAS) [14].

2. Materials and methods

2.1. Cloning, expression and purification

The *ton1374* gene (GenBank accession No. 7018405) was amplified by polymerase chain reaction (PCR) using *T. onnurineus* NA1 genomic DNA as the template [15]. The gene was inserted downstream of the T7 promoter in the expression plasmid pET-24a (Novagen), and the resulting construct expressed residues 2–261 of the TON1374 protein with an in-frame non-cleavable N-terminal His_6 tag (MHHHHHH). After verifying the DNA sequence, plasmid DNA was transformed into *Escherichiacoli* strain Rosetta (DE3) pLys (Stratagene). The cells were grown to an OD_{600} of approximately 0.5 in Luria–Bertani medium containing 50 μg/ml kanamycin (Duchefa) at 310 K, and expression was induced by 1 mM isopropyl-β-D-thiogalactoside (IPTG, Duchefa). After 12 h induction at 295 K, the cells were harvested and resuspended in 20 mM Tris–HCl pH 7.5 (Duchefa), containing 500 mM sodium chloride and 5 mM imidazole. The cells were disrupted by sonication, and the cell debris was discarded by centrifugation at 20000 g for 30 min at 277 K. The resulting supernatant was loaded onto a nickel-nitrilotriacetic acid (Ni–NTA) column (Qiagen). The column was washed with a buffer containing 20 mM Tris–HCl pH 7.5, 500 mM NaCl, and 30 mM imidazole. TON1374 was eluted with the same buffer containing 500 mM imidazole. The protein fraction partially purified by Ni–NTA was concentrated and subsequently loaded onto a Superdex 75 HR 16/60 column (GE Healthcare) pre-equilibrated with a buffer containing 20 mM Tris–HCl pH 7.5, 300 mM NaCl, and 1 mM DTT. The TON1374 protein eluted at ~31.3 min and ~38.9 min at a flow rate of 1.5 ml/min. The purified TON1374 was concentrated to approximately 25 mg/ml for crystallization. For the SeMet labeling of TON1374, the *E. coli met*$^-$ auxotrophic strain B834 (DE3) (Novagen) was used as a host for plasmid transformation. Cells were grown to an OD_{600} of approximately 0.5 in M9 medium including 50 mg/l of SeMet and 50 μg/ml kanamycin at 310 K, and expression was induced by 1 mM IPTG at 295 K. The cells were harvested after 12 h. SeMet TON1374 was purified by same procedures as for the native TON1374 protein. Purified SeMet TON1374 was concentrated to approximately 25 mg/ml for crystallization.

2.2. Crystallization and data collection

Crystals of SeMet TON1374 were grown at 295 K using the batch crystallization method with a mother liquor of 1.5 M sodium nitrate and 0.1 M sodium acetate pH 4.5. For data collection at a cryogenic temperature, the crystals were transferred to a solution containing 4.5 M sodium nitrate and 5% PEG 200. This step appeared to be very sensitive as the crystals were disrupted if transferred directly to the cryoprotectant buffer. Thus, to prevent such disruption, the concentration of sodium nitrate was increased gradually by 0.5 M intervals. The crystal was frozen at 100 K after brief immersion in a final cryoprotectant solution. A 2.58 Å SAD data set (Table 1) was collected at wavelengths of 0.97884 Å using an ADSC Quantum 270 CCD on the microfocus beamline 17A at the Photon Factory, Japan.

Apo TON1374 was grown at 295 K using the batch crystallization method with a mother liquor of 0.16 M magnesium chloride hexahydrate, 0.08 M Tris–HCl pH 8.5, and 24% (w/v) polyethylene glycol 4,000. Crystals of the TON1374/ATP complex were obtained by soaking apo crystals into a solution containing 0.16 M magnesium chloride hexahydrate, 0.08 M Tris–HCl pH 8.5, 24% (w/v) polyethylene glycol 4,000, and 4 mM ATP. After soaking for 1 h, a complex crystal was mounted and the crystal was frozen at 100 K without additional cryoprotectant. A 1.96 Å resolution apo TON1374 data set was collected at a wavelength of 1.00 Å using an ADSC Quantum 315r CCD on beamline BL-5C at the Pohang Light Source, Republic of Korea (Table 1). A 2.19 Å TON1374/ATP complex data set was collected at a wavelength of 0.98 Å using an ADSC Quantum 270 CCD on microfocus beamline BL-17A at the Photon Factory, Japan (Table 1).

Table 1
Data collection and Refinement.

Data sets, Space group	SeMet TON1374 SAD, $P4_12_12$	TON1374 Apo, *C*2	TON1374/ATP complex *C*2
Wavelength (Å)	0.97884	1.00000	0.98000
Resolution (Å)	50–2.58	50–1.96	50–2.19
Completeness (%)[a]	98.5(97.3)	96.7(89.2)	97.8(92.7)
R_{merge} (%)[a,b]	8.9(46.1)	5.9(32.3)	7.4(34.1)
Average I/σ[a]	29.4(2.9)	28.6(2.3)	28.6(3.5)
Refinement statistics			
Resolution range (Å)		33.26–1.96	37.62–2.19
Number of atoms			
Water		275	185
Acetate		2	
Magnesium			2
ATP			4
R_{work} /R_{free} (%)[c]		21.6/26.8	21.0/26.0
R.m.s. deviations[d]			
Bonds (Å)		0.017	0.015
Angles (°)		1.881	1.706

[a] The number in parentheses is for the outer shell.
[b] $R_{merge} = \Sigma_{hkl} \Sigma_i |I_i(hkl) - \langle I(hkl)\rangle| / \Sigma_{hkl} \Sigma_i I_i(hkl)$, where $I_i(hkl)$ is the intensity of observed reflection *hkl* and $\langle I(hkl)\rangle$ is the mean intensity of symmetry-equivalent reflections.
[c] $R_{work} = \Sigma_{hkl} \; ||F_{obs}|-F_{cale}|| / \Sigma_{hkl} |F_{obs}|$. R_{free} was calculated with 5% of the reflections.
[d] R.m.s. deviations in bond length and angles are the deviations from ideal values.

2.3. Data processing, structure determination and refinement

All the data were integrated and scaled with HKL2000 [16]. The selenium substructures of SeMet TON1374 were located, and the phases were calculated using the PHENIX program suite [17]. The subsequent solvent flattening resulted in an interpretable map and a traceable autobuilt model. The structures of apo TON1374 and TON1374/ATP complex were determined by molecular replacement using MOLREP [18] in the CCP4 program suite [19] with the initial SeMet TON1374 structure as a search model. Additional model building was performed using COOT [20], and refinement was performed with the maximum likelihood algorithm implemented in CNS [21] and with REFMAC [22]. The ideality of the stereochemistry of the final models was verified by PROCHECK [23]. The Ramachandran plots indicate that 90.9% (TON1374) and, 92.9% (TON1374/ATP complex) of the non-glycine residues are in the most favored regions and that the remaining 8.2% (TON1374) and, 6.5% (TON1374/ATP complex) residues are in allowed regions. All figures were prepared using PyMOL (http://pymol.sourceforge.net/).

2.4. PDB accession numbers

The atomic coordinates and structure factors of apo-form and ATP complex of TON1374 have been deposited in the Protein Data Bank, with the accession code 4MB0 and 4MB2, respectively.

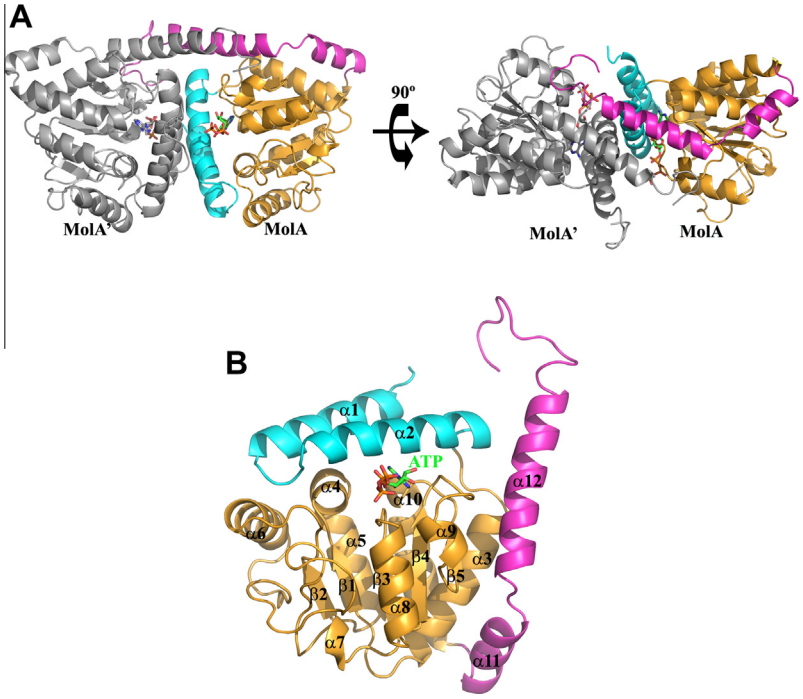

Fig. 1. Overall structure of TON1374. (A) The dimeric structure of the TON1374/ATP complex is presented as a ribbon diagram. MolA and MolA′ (grey) represent each subunit of the dimer. For clarity, the lid domain (cyan), the core domain (orange), and C-terminal two α-helices (brick) in MolA are differently colored. ATP molecules are in sticks. (B) The monomeric structure of the TON1374/ATP complex is presented as a ribbon diagram with secondary structures labeled. (For interpretation of the references to color in this figure legend, the reader is referred to the web version of this article.)

3. Results and discussion

3.1. Overall structure

Single-wavelength anomalous dispersion data at a 2.58 Å resolution was collected at the selenium absorption peak to solve the TON1374 structure *de novo*. SeMet crystals of apo TON1374 belong to the space group $P4_12_12$, with two molecules in the asymmetric unit consisting of one TON1374 dimer. The crystal structures of the apo TON1374 protein and its ATP complex were solved by molecular replacement using the initial SeMet TON1374 structure as a search model at 1.96 Å and 2.19 Å resolutions, respectively (Table 1). The apo TON1374 and TON1374/ATP complex crystals belong to the space group *C*2, with four molecules in the asymmetric unit consisting of two TON1374 dimers (Fig. 1A).

The TON1374 monomer adopts a two-domain structure composed of an N-terminal lid domain (residues 1–49) and a core α/β domain (residues 50–216) followed by two C-terminal helices (217–261) (Fig. 1B). The N-terminal lid domain consists of two α-helices (α1, α2). The core α/β domain has a central five-stranded parallel β-sheet (β1– β5), of an ↑β2 - ↑β1 - ↑β3 - ↑β4 - ↑β5 arrangement, with three α-helices on one face (α3, α5, α10), one 3_{10}-helix and two α-helices on the other face (α7, α8, α9), and two α-helices on top (α4, α6) (Fig. 1B). Superimpositions of the corresponding C^{α} atoms among the four subunits in the apo and ATP complex structures of TON1374 gave r.m.s.d. values in the range of 0.31–0.36 Å and 0.19–0.30 Å, respectively. Superimposition of the corresponding C^{α} atoms between the apo and ATP complex structures gave an r.m.s.d. value of 0.14 Å. These results showed that there were little structural differences among the four subunits in the asymmetric unit and that ATP-binding has little effect on the overall protein conformation. Structural homolog search using the DALI server revealed that the core domain of TON1374 has limited similarity to the nucleotide binding α/β domains or Rossmann fold-like domains of some enzymes including *Oxalobacter formigenes* oxalyl-CoA decarboxylase with the highest Z-score of 13.8 [12] (Fig. S2).

3.2. Dimerization

The dimer of TON1374 resembles a butterfly when viewed from one side (Fig. 1A and Fig. 2A). The dimer interface is extensive, with the apo enzyme having an interface area of ~2053 Å^2 and with the ATP complex having an interface area of ~2025 Å^2, as calculated using the PISA server [24]. The lid domain and the C-terminal α12 helix are implicated in the dimeric contact, forming a fan-shaped interface (Fig. 2B and Fig. 2C). The dimer contact is maintained mainly via hydrophobic interactions from the α2 and α12 helices of each subunit. Leu34 and Ile35 of α2 and Leu34′ and Ile35′ of α2′ (hereafter, prime denotes the other subunit in the dimer) make a hydrophobic contact point from which α2 and α2′ expand toward the arc region that consists of the α12 and α12′ helices. Ala42, Phe43, and Leu46 in α2 and Ala42′, Phe43′, and Leu46′ in α2′ form a highly extensive hydrophobic core, which is completed by additional hydrophobic residues from α12 and α12′ (Leu239, Ile242, Leu246, Leu249, Leu239′, Ile242′, Leu246′, and Leu249′) (Fig. 2B).

The dimer contact is further stabilized by hydrogen bonds and electrostatic interactions between the α12 and α12′ helices that surround the hydrophobic core. The interaction pairs are as follows: the side-chain hydroxyl group of Thr247 with the side-chain guanidinium group of Arg243′; the back-bone carbonyl oxygen of Ala250 with the side-chain amino group of Asn236′; the side-chain guanidinium group of Arg256 with the side-chain carboxyl group of Asp193′ and the back-bone carbonyl oxygen of Met191′; the indole nitrogen of Trp255 with the back-bone carbonyl oxygen of Ala192′; and the back-bone carbonyl oxygen of Ile254 with the side-chain guanidinium group of Arg190′. There are also three polar interactions between α2 and α12 (identical to α2′ and α12′) and one polar interaction between α2 and α2′. The side-chain

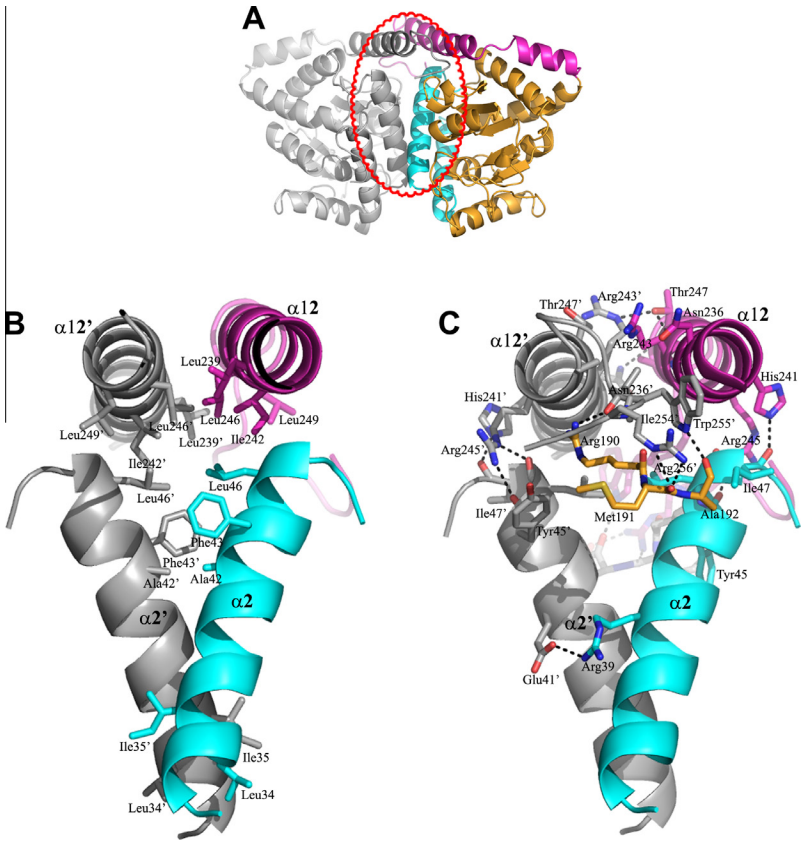

Fig. 2. Dimerization interface. (A) The left image of the TON1374 dimer in Fig. 1A is slightly rotated to show the dimerization interface clearly. A red circled region is magnified in (B) and (C). (B) Hydrophobic interactions in the dimerization interface of TON1374. (C) Polar interactions in the dimerization interface of TON1374 are indicated by dotted lines. All colors in Fig. 2 are same as in Fig. 1. (For interpretation of the references to color in this figure legend, the reader is referred to the web version of this article.)

guanidinium group of Arg245 in α12 exhibits polar interactions with the back-bone carbonyl oxygen atoms of Tyr45 and Leu46 in α2. The side-chain imidazole nitrogen of His241 in α12 shows polar interaction with the back-bone carbonyl oxygen of Ile47 in α2, and the side-chain guanidinium group of Arg39 in α2 shows polar interaction with the side-chain carboxyl group of Glu41′ in α2′ (Fig. 2C).

3.3. The ATP binding site

The TON1374/ATP complex structure reveals an ATP molecule bound to the pocket between the lid and core domains of TON1374, with the triphosphate group pointing toward the dimer interface. All four subunits in the asymmetric unit are occupied by ATP molecules. Because all the interactions between the adenosine moiety and TON1374 are identical, for convenience, we describe only the ATP binding site in molecule A, which shows the best electron density map quality. The adenine plane is sandwiched between the hydrophobic side-chains, notably Leu161 and Leu182. The base is stabilized by a hydrogen-bonding pattern reminiscent of Watson–Crick base pairing, consisting of two hydrogen bonds between N6 and the side-chain oxygen of Asn199 and N1 and the amide nitrogen of Ile200. In addition, there are two more hydrogen bonds between N3 and the amide nitrogen of Leu182, N7 and one conserved water molecule. The ribose ring is further stabilized by a pair of interactions between the side-chain carboxyl group of Asp181 and O2′ and O3′ of the sugar moiety (Fig. 3A).

Although the hydrogen bonding networks are conserved in the adenine and ribose binding sites, the triphosphate binding site has a conformational plasticity among the four subunits. The side-chain guanidinium group of Arg39 in the α2 helix forms hydrogen bonds with O atoms in the α- or β-phosphate groups, and the side-chain guanidinium group in Arg17′ from α2′ forms hydrogen bonds with O atoms in the β- or γ-phosphate groups (Fig. 3A). In addition, the side-chain carboxyl group of Asp163 makes hydrogen bonds with O atoms in the γ-phosphate group when Arg39 and Asn17′ form hydrogen bonds with O atoms in the α- and β-phosphate groups (Fig. 3A). In two of the four subunits, we also observed that the hydroxyl group of Tyr45′ forms hydrogen bonds with O atoms in β- or γ-phosphate groups (Fig. 3A). So, the surface exposed triphosphate binding sites and the flexible side-chains participating in hydrogen bonds are the reason for the conformational plasticity of the triphosphate binding mode. Interestingly, all of the residues that participate in the hydrogen bond networks with ATP, are strictly conserved in the archaeal PPS homolog (Fig. S1).

The higher selectivity of PPS for ATP, i.e., no activity was detected with other NTPs [8], can be explained by an asparagine (Asn199 in TON1374) which has the highest propensity for adenine binding sites [25]. The N6 atom of adenine makes a hydrogen bond with the side-chain carbonyl oxygen of Asn199. Because the orientation of the side-chain rotamer in Asn199 is tightly maintained by a series of polar interactions among Asp198, Arg202, and Asp44, O6 atom of the guanine moiety of GTP should face the charge repulsion. In addition, histidine (His37 in TON1374) is known to be much more favored in the adenine environment where it is often involved in stacking interactions with the adenine rings [25] (Fig. 3A).

3.4. Proposed 4-phosphopantoate binding site

PPS catalyzes the archaea-specific condensation reaction of 4-phosphopantoate and β-alanine using ATP to produce 4′-phospho-

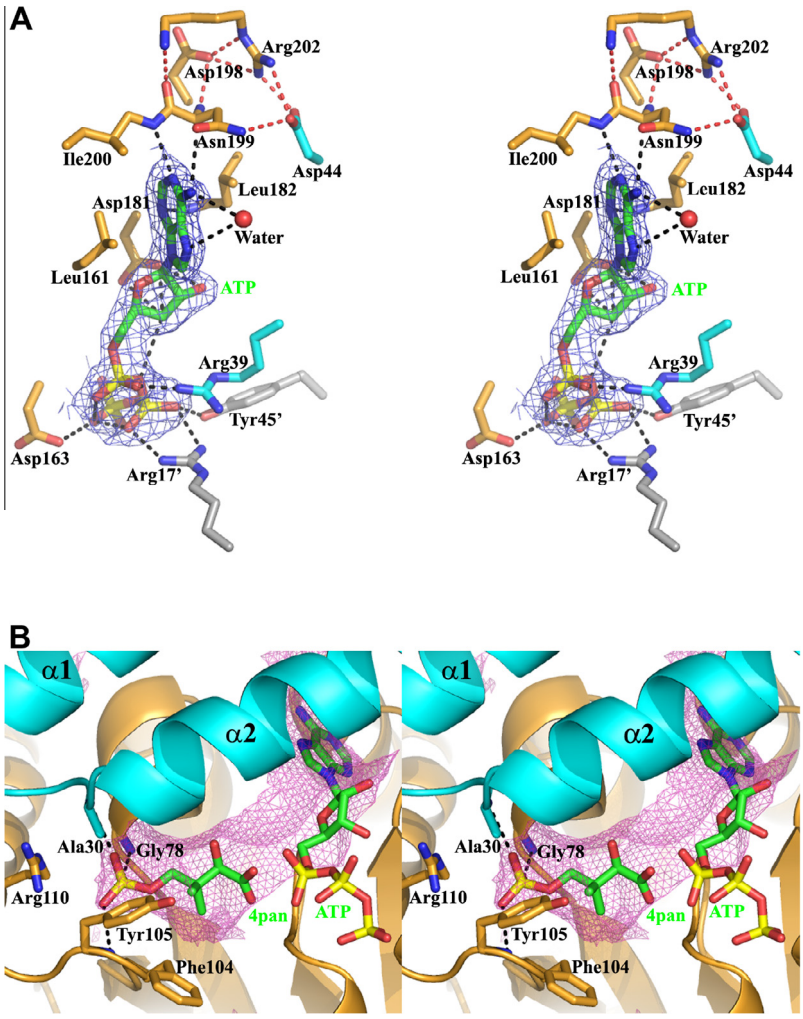

Fig. 3. ATP-binding site and proposed 4-phosphopantoate binding site. (A) Stereo diagram of the ATP-binding site. ATP molecules (green) and interacting residues are shown in sticks. A conserved water molecule making a hydrogen bond with N6 atom is represented as a red sphere. Black dotted lines indicate polar interactions between ATP and TON1374, and polar interactions that stabilize the rotameric conformation of Asn199 are represented as red dotted lines. (B) 4-phosphopantoate (4pan) binding site is proposed by using the molecular docking server, PatchDock. A solvent accessible cavity accommodating ATP and 4pan is presented as a violet mesh. 4pan and ATP are colored in green, and the residues involved in 4pan binding are shown in sticks. All colors in Fig. 3 are same as in Fig. 1. (For interpretation of the references to color in this figure legend, the reader is referred to the web version of this article.)

pantothenate. This reaction may proceed through the 4-phosphopantoyl adenylate intermediate which is formed by the nucleophilic attack of the carboxyl group in 4-phosphopantoate on the phosphorus of α-phosphate in ATP just like the bacterial PS enzyme reaction [26]. In this respect, we assumed that 4-phosphopantoate would bind in the proximity of ATP with its carboxyl group near the α-phosphate and its phosphate group near the positively charged surface area. We found a cavity of solvent-accessible area of a size similar to 4-phosphopantoate immediately adjacent to the ATP binding site. Using the automated molecular docking server PatchDock [27], we successfully localized 4-phosphopantoate to this area. In our model, the carboxyl group of 4-phosphopantoate faces α-phosphate of ATP, and the phosphate group makes hydrogen bonds with backbone amide nitrogen atoms of Ala30, Gly78, and Tyr105 (Fig. 3B). And, the positively charged Arg110 is close enough to engage in polar contact with the phosphate group of 4-phosphopantoate. In addition, Phe104 and Tyr105 further stabilize the binding of 4-phosphopantoate by establishing a hydrophobic platform for the dimethyl group of 4-phosphopantoate (Fig. 3B).

However, molecular docking of β-alanine to the TON1374/ATP/4-phosphopantoate complex model failed to obtain the proper model, which appeared to be caused by the absence of the additional surface area for β-alanine to be located in the active site with ATP and 4-phosphopantoate at the same time. Thus, β-alanine may enter the active site and attack the α-phosphate atom of 4-phosphopantoyl adenylate intermediate after the pyrophosphate is released.

Acknowledgments

We thank the beamline staff at BL-5C, PLS, Republic of Korea and BL-17A, PF, Japan for support with the data collection. This work was supported by the National Research Foundation of Korea Grant (NRF-2012R1A2A2A02005978), the Marine and Extreme Genome Research Center program and the Development of Biohydrogen Production Technology Using Hyperthermophilic Archaea program of MLTM, and the KIOST in-house NSC program.

Appendix A. Supplementary data

Supplementary data associated with this article can be found, in the online version, at http://dx.doi.org/10.1016/j.bbrc.2013.09.008.

References

[1] H. Kleinkauf, The role of 4′-phosphopantetheine in the biosynthesis of fatty acids, polyketides and peptides, Biofactors 11 (2000) 91–92.
[2] C.M. Smith, W.O. Song, Comparative nutrition of pantothenic acid, Journal of Nutritional Biochemistry 7 (1996) 312–321.
[3] S.L. Miller, G. Schlesinger, Prebiotic syntheses of vitamin coenzymes: II, Pantoic acid, pantothenic acid, and the composition of coenzyme A, J Mol Evol 36 (1993) 308–314.
[4] U. Genschel, Coenzyme A biosynthesis: Reconstruction of the pathway in archaea and an evolutionary scenario based on comparative genomics, Molecular Biology and Evolution 21 (2004) 1242–1251.
[5] S. Ronconi, R. Jonczyk, U. Genschel, A novel isoform of pantothenate synthetase in the Archaea, Febs Journal 275 (2008) 2754–2764.
[6] Y. Yokooji, H. Tomita, H. Atomi, T. Imanaka, Pantoate kinase and phosphopantothenate synthetase, two novel enzymes necessary for CoA biosynthesis in the Archaea, J Biol Chem 284 (2009) 28137–28145.
[7] H. Tomita, Y. Yokooji, T. Ishibashi, T. Imanaka, H. Atomi, Biochemical characterization of pantoate kinase, a novel enzyme necessary for coenzyme A biosynthesis in the Archaea, J Bacteriol 194 (2012) 5434–5443.
[8] T. Ishibashi, H. Tomita, Y. Yokooji, T. Morikita, B. Watanabe, J. Hiratake, A. Kishimoto, A. Kita, K. Miki, T. Imanaka, H. Atomi, A detailed biochemical characterization of phosphopantothenate synthetase, a novel enzyme involved in coenzyme A biosynthesis in the Archaea, Extremophiles 16 (2012) 819–828.
[9] R.D. Finn, J. Mistry, J. Tate, P. Coggill, A. Heger, J.E. Pollington, O.L. Gavin, P. Gunasekaran, G. Ceric, K. Forslund, L. Holm, E.L. Sonnhammer, S.R. Eddy, A. Bateman, The Pfam protein families database, Nucleic Acids Res 38 (2010) D211–D222.
[10] A. Bateman, P. Coggill, R.D. Finn, DUFs: families in search of function, Acta Crystallogr Sect F Struct Biol Cryst Commun 66 (2010) 1148–1152.
[11] R.L. Tatusov, E.V. Koonin, D.J. Lipman, A genomic perspective on protein families, Science 278 (1997) 631–637.
[12] C.L. Berthold, C.G. Toyota, P. Moussatche, M.D. Wood, F. Leeper, N.G. Richards, Y. Lindqvist, Crystallographic snapshots of oxalyl-CoA decarboxylase give insights into catalysis by nonoxidative ThDP-dependent decarboxylases, Structure 15 (2007) 853–861.
[13] J.L. Avalos, J.D. Boeke, C. Wolberger, Structural basis for the mechanism and regulation of Sir2 enzymes, Mol Cell 13 (2004) 639–648.
[14] M.E. Caines, J.M. Elkins, K.S. Hewitson, C.J. Schofield, Crystal structure and mechanistic implications of N2-(2-carboxyethyl)arginine synthase, the first enzyme in the clavulanic acid biosynthesis pathway, J Biol Chem 279 (2004) 5685–5692.
[15] H.S. Lee, S.G. Kang, S.S. Bae, J.K. Lim, Y. Cho, Y.J. Kim, J.H. Jeon, S.S. Cha, K.K. Kwon, H.T. Kim, C.J. Park, H.W. Lee, S.I. Kim, J. Chun, R.R. Colwell, S.J. Kim, J.H. Lee, The complete genome sequence of Thermococcus onnurineus NA1 reveals a mixed heterotrophic and carboxydotrophic metabolism, J Bacteriol 190 (2008) 7491–7499.
[16] Z. Otwinowski, W. Minor, Processing of X-ray diffraction data collected in oscillation mode, Macromolecular Crystallography, Pt A 276 (1997) 307–326.
[17] P.D. Adams, P.V. Afonine, G. Bunkoczi, V.B. Chen, I.W. Davis, N. Echols, J.J. Headd, L.W. Hung, G.J. Kapral, R.W. Grosse-Kunstleve, A.J. McCoy, N.W. Moriarty, R. Oeffner, R.J. Read, D.C. Richardson, J.S. Richardson, T.C. Terwilliger, P.H. Zwart, PHENIX: a comprehensive Python-based system for macromolecular structure solution, Acta Crystallogr D Biol Crystallogr 66 (2010) 213–221.
[18] A. Vagin, A. Teplyakov, Molecular replacement with MOLREP, Acta Crystallogr D Biol Crystallogr 66 (2010) 22–25.
[19] M.D. Winn, C.C. Ballard, K.D. Cowtan, E.J. Dodson, P. Emsley, P.R. Evans, R.M. Keegan, E.B. Krissinel, A.G. Leslie, A. McCoy, S.J. McNicholas, G.N. Murshudov, N.S. Pannu, E.A. Potterton, H.R. Powell, R.J. Read, A. Vagin, K.S. Wilson, Overview of the CCP4 suite and current developments, Acta Crystallogr D Biol Crystallogr 67 (2011) 235–242.
[20] P. Emsley, K. Cowtan, Coot: model-building tools for molecular graphics, Acta Crystallogr D Biol Crystallogr 60 (2004) 2126–2132.
[21] A.T. Brunger, P.D. Adams, G.M. Clore, W.L. DeLano, P. Gros, R.W. Grosse-Kunstleve, J.S. Jiang, J. Kuszewski, M. Nilges, N.S. Pannu, R.J. Read, L.M. Rice, T. Simonson, G.L. Warren, Crystallography & NMR system: A new software suite for macromolecular structure determination, Acta Crystallogr D Biol Crystallogr 54 (1998) 905–921.
[22] G.N. Murshudov, A.A. Vagin, E.J. Dodson, Refinement of macromolecular structures by the maximum-likelihood method, Acta Crystallogr D Biol Crystallogr 53 (1997) 240–255.
[23] R.A. Laskowski, M.W. Macarthur, D.S. Moss, J.M. Thornton, Procheck - a Program to Check the Stereochemical Quality of Protein Structures, Journal of Applied Crystallography 26 (1993) 283–291.
[24] E. Krissinel, K. Henrick, Inference of macromolecular assemblies from crystalline state, J Mol Biol 372 (2007) 774–797.
[25] I. Nobeli, R.A. Laskowski, W.S. Valdar, J.M. Thornton, On the molecular discrimination between adenine and guanine by proteins, Nucleic Acids Res 29 (2001) 4294–4309.
[26] F. von Delft, A. Lewendon, V. Dhanaraj, T.L. Blundell, C. Abell, A.G. Smith, The crystal structure of E. coli pantothenate synthetase confirms it as a member of the cytidylyltransferase superfamily, Structure 9 (2001) 439–450.
[27] D. Schneidman-Duhovny, Y. Inbar, R. Nussinov, H.J. Wolfson, PatchDock and SymmDock: servers for rigid and symmetric docking, Nucleic Acids Res 33 (2005) W363–W367.